Water Exchange across Isobaths over the Continental Shelf of the East China Sea

JING ZHANG

Key Laboratory of Physical Oceanography, Ocean University of China, Ministry of Education China, Qingdao, China, and Center for Marine Environmental Studies, Ehime University, Matsuyama, Japan

XINYU GUO

Center for Marine Environmental Studies, Ehime University, Matsuyama, and Application Laboratory, Japan Agency for Marine-Earth Science and Technology, Yokohama, Japan, and Key Laboratory of Marine Environment and Ecology, Ocean University of China, Ministry of Education, Qingdao, China,

LIANG ZHAO

College of Marine and Environmental Sciences, Tianjin University of Science and Technology, Tianjin, China

YASUMASA MIYAZAWA

Application Laboratory, Japan Agency for Marine-Earth Science and Technology, Yokohama, Japan

QUN SUN

College of Marine and Environmental Sciences, Tianjin University of Science and Technology, Tianjin, China

(Manuscript received 16 October 2016, in final form 28 January 2017)

ABSTRACT

Onshore and offshore currents and the associated volume transport across three isobaths (50, 100, and 200 m) over the continental shelf of the East China Sea were examined using daily reanalysis data in 1993–2012. After being averaged along the isobaths, the velocities across 100 and 50 m are onshore in the bottom layer but offshore in the surface layer. In contrast, those across the 200-m isobath are onshore in the surface and bottom layers but without a clear direction in the midlayer, suggesting a three-layer structure. The surface offshore current across the 100-m isobath mainly arises from the Taiwan Strait Current, while the surface onshore current across the 200-m isobath mainly arises from the Kuroshio, both of which converge in the area between the 100- and 200-m isobaths and flow toward the Tsushima Strait. The control of bottom Ekman dynamics on the onshore bottom currents is important at the 100-m isobath, partly important at the 200-m isobath, and slightly important at the 50-m isobath. The seasonal variations of onshore and offshore currents in the surface layers across the three isobaths are likely caused by local winds, the Taiwan Strait Current, and the Changjiang discharge, while those in midlayer across the 200-m isobath demonstrate a strong geostrophic control and can be interpreted from a traditional viewpoint on the Kuroshio intrusion over the entire water column across the shelf slope. The close connection of bottom onshore currents across the three isobaths suggests that the bottom layer is an important pathway for water exchange of shelf water and the open sea.

1. Introduction

The East China Sea (ECS) is a marginal sea of the northwest Pacific Ocean and has one of the largest continental shelves in the world. The Kuroshio, a western boundary current in the North Pacific Ocean, enters the ECS from the northeast of Taiwan. The main flow extends northeastward along the shelf break and a portion is diverted from the constraint of steep topography and intrudes onto the ECS shelf. Through exchanges with shelf water along the shelf break, which is usually denoted by the 200-m isobath, the Kuroshio transports large amounts of heat, salt, and nutrients onto the shelf (Chen and Wang 1999; Hsueh 2000; Fang et al. 2003; Zhang et al. 2007). The exchange between Kuroshio and ECS shelf

Corresponding author e-mail: Xinyu Guo, guoxinyu@sci.ehime-u.ac.jp

DOI: 10.1175/JPO-D-16-0231.1

water plays a large role in continental shelf circulation (Hsueh et al. 1997; Ma et al. 2010) and the associated ecosystems (Zhao and Guo 2011) in the ECS.

The Kuroshio intrudes onto the shelf mainly at two locations: northeast of Taiwan and southwest of Kyushu. In the area northeast of Taiwan, the Kuroshio loses the support of the Taiwan Island and intrudes onto the shelf because of the geostrophic adjustment (Su 2001). Some of the intruded water, which is considered the Kuroshio Branch Current north of Taiwan (KBCNT), returns to the main stream because of the bottom friction and the topographic beta effect (Qiu and Imasato 1990; Su 2001). The other intruded water goes farther into the ECS shelf. Yang et al. (2011, 2012) proposed that a nearshore Kuroshio bottom branch current could upwell gradually from the shelf break to the continental shelf offshore of the Changjiang estuary in summer.

When the Kuroshio main stream reaches the southwest of Kyushu, it turns clockwise to the east and leaves the ECS through the Tokara Strait. As a result of the conservation of potential vorticity, another Kuroshio Branch Current west of Kyushu (KBCWK) forms and intrudes shoreward (Hsueh et al. 1996; Lie et al. 1998; Hsueh 2000; Isobe 2000).

Besides the KBCNT and KBCWK, the onshore intrusion of the Kuroshio along the entire shelf break has been gaining more attention recently through both observations and numerical models. Teague et al. (2003) computed volume transports across the Taiwan and Tsushima Straits through direct velocity measurements. Based on the difference between the two straits, they estimated that the volume transport across the entire shelf break was about 3 Sv (1 Sv $\equiv 10^6\,\mathrm{m^3\,s^{-1}}$) onshore from October to December. Guo et al. (2006) used a nested ocean model and obtained a mean Kuroshio onshore transport of 1.46 Sv across the shelf break of the ECS (denoted by the 200-m isobath). Isobe (2008) reported an annual-mean transport of 1.4 Sv based on the summation of all available volume transport values through the Taiwan Strait and Tsushima Strait in the literatures.

The Kuroshio onshore transport has a strong seasonal variation, showing a maximum in autumn and a minimum in summer (Teague et al. 2003; Guo et al. 2006; Isobe 2008; Oey et al. 2010; Wu et al. 2014). Strong seasonal variation in the Kuroshio onshore transport is associated with the monsoon and the changes in the density field (Chao 1990; Guo et al. 2006) as well as volume transport through the Taiwan Strait and Kuroshio transport east of Taiwan (Lee and Matsuno 2007). Changes in the density field are further linked to the combined effects of surface heat flux and the monsoon (Oey et al. 2010; Wu et al. 2014).

In addition to seasonal fluctuations, the long-term variability of Kuroshio onshore intrusion has also been studied (Liu et al. 2014; Wu et al. 2014). Based on model results, Liu et al. (2014) reported that the interannual variation of Kuroshio onshore intrusion was as prominent as its seasonal variation and had a period of 4 yr that also appears in the volume transport of Kuroshio itself. Based on multisatellite geostrophic velocity data, Wu et al. (2014) reported that the interannual variations of the Kuroshio intrusion northeast of Taiwan in winter was related to the surface heat flux gradient (positively correlated) and upstream Kuroshio transport (negatively correlated) rather than the local winds.

Although the Kuroshio onshore transport was emphasized in previous studies, shelf water is also known to be present in the main stream of the Kuroshio. Isobe et al. (2004) observed less saline shelf water in the Kuroshio subsurface layer (~100-m depth) around the shelf break of the ECS. Therefore, the water movement across the shelf break of the ECS must occur in two directions: onshore and offshore. The Kuroshio onshore transport reported in previous studies is actually the combined result of onshore and offshore transport. For this reason, it is a net volume transport across the shelf break.

Net volume transport alone cannot fully account for the actual water exchange process that occurs essentially in two directions, although it can be evaluated by the differences in volume transport through the Taiwan Strait and Tsushima Strait (Teague et al. 2003). On the other hand, the onshore and offshore water movements occur not only at the shelf break (usually at the 200-m isobath in previous studies) but also over the ECS shelf where the water depth is less than 200 m. Therefore, we also need to examine the water exchange processes between the inner shelf (<50 m) and midshelf (50–100 m) and between the midshelf and outer shelf (100–200 m) in the ECS.

The documentation of onshore and offshore transports is also of great significance to understand the material transport between the open ocean and shelf seas. Material concentration in water flowing onshore is usually different from that in water flowing offshore. For example, nutrient concentrations have an apparent horizontal gradient from coastal water to the Kuroshio in the ECS (Zhang et al. 2007). Consequently, the mean dissolved inorganic nitrogen concentration in the water flowing onshore across the 200-m isobath was smaller (larger) than that in the water flowing offshore from September to the following March (from April to September; Zhao and Guo 2011). Since the onshore and offshore volume transports across the 200-m isobath in the ECS are larger than the net volume transport by one

order of magnitude, the difference in the nutrient concentration in the water flowing onshore and offshore is important to the nutrient budget in the ECS. Furthermore, the documentation of the offshore transport is helpful to understand the transport of terrestrial material to the open sea. Based on measurements in the ECS, Ren et al. (2015) suggested that the offshore transport of terrestrial material contributed to the northward increase of dissolved aluminum in the upper regions of the 100-m isobath along the shelf break.

In this study, we focus on the dynamics related to water exchange between the inner shelf (<50 m) and midshelf (50–100 m), between the midshelf and outer shelf (100–200 m), and between the outer shelf and the Kuroshio region (>200 m) over the continental shelf of the ECS. Based on reanalysis data, we calculated net, onshore, and offshore volume transports across the 200-, 100- and 50-m isobaths in the ECS with special attention to spatial and temporal variations in the cross-isobath currents. We also discuss the controlling factors in the seasonal variations of net volume transports in different vertical layers. Section 2 gives a brief description and validation of the reanalysis data as well as the calculation method of volume transport across three isobaths (50, 100, and 200 m). Section 3 presents the mean states of currents and volume transports across the three isobaths as well as spatial and temporal variations. Section 4 gives an analysis on the mechanisms controlling the seasonal variations in volume transport at different water depths. Section 5 discusses the connections among the three isobaths and summarizes this study.

2. Reanalysis data

The reanalysis data were obtained by a data assimilative ocean model developed by the Japan Coastal Ocean Predictability Experiment (JCOPE2; Miyazawa et al. 2009). The ocean model in the JCOPE2 system is based on the Princeton Ocean Model with a generalized sigma coordinate (POMgcs; Mellor et al. 2002). A high-resolution regional model (10.5°–62°N, 108°–180°E) with spatial grid resolution of 1/12° and 46 vertical levels was embedded in a low-resolution model (30°S–62°N, 100°E–90°W) with a spatial grid resolution of approximately 1/4° and 21 sigma levels, covering almost the entire Pacific region, using the one-way nesting method.

The model was driven by wind stresses and heat and salt fluxes. Wind stress and heat flux fields were calculated from the 6-hourly National Centers for Environmental Prediction–National Center for Atmospheric Research (NCEP–NCAR) reanalysis data (Kalnay et al. 1996) using bulk formulas (Kagimoto et al. 2008). The wind stress was multiplied by a factor of 0.7 to adjust the Kuroshio transport south of Japan (Hirose 2011). Runoff of Changjiang was included as the only river discharge into the model domain. It is worth mentioning that a tidal mixing scheme based on the amplitude of tidal currents (Lee and Matsuno 2007) was added when calculating the eddy viscosity in the model in order to improve the simulation of the circulation in the ECS, where tide plays a certain role in the formation and movement of water mass.

The following observation data were used for data assimilation in the JCOPE2 model: along-track sea surface height anomaly (SSHA) obtained from the TOPEX/Poseidon and *ERS-1* and *ERS-2* satellites during the period December 1992 to January 2002 and from the *Jason-1* and *Geosat Follow-On* during the period January 2002 to January 2008; sea surface temperature (SST) obtained from the Advanced Very High Resolution Radiometer (AVHRR)/multichannel sea surface temperature (MCSST) products; and vertical profiles of temperature and salinity obtained from the data archive of the Global Temperature and Salinity Profile Program (GTSPP).

The JCOPE2 used three-dimensional variational data assimilation (3DVAR) to construct its data assimilation system that is mainly designed for the Kuroshio region and subtropical ocean [more details on the assimilation method can be found in Miyazawa et al. (2009)]. In the ECS, besides introducing Changjiang runoff and tidal mixing effects, the JCOPE2 assimilates SST over it. Since the JCOPE2 assimilates the data of water temperature and salinity but solves the momentum equation without assimilation, the dynamics in the momentum equation are physical consistence.

The low-resolution and high-resolution models were spun up for 15 and 5 yr, respectively. Reanalysis calculations from November 1992 were carried out for both models with the data assimilation and the external forcing. The daily mean of SSH, two horizontal velocity components, water temperature, and salinity from 1993 to 2012 were provided for our study.

The bathymetry of JCOPE2 in the ECS is shown in Fig. 1. We designated three isobaths for examining water exchange between the inner and midshelf by using the 50-m isobath, between the mid- and outer shelf by using the 100-m isobath, and between the outer shelf and the Kuroshio by using the 200-m isobath. The grid points of the 100- and 200-m isobaths generally follow their water depths. For purposes of easily considering water budget, we extended the grid points of the 50-m isobath to the coastline. The four seasons were given according to the common usage in the ECS: spring from March to May, summer from June to August, autumn from

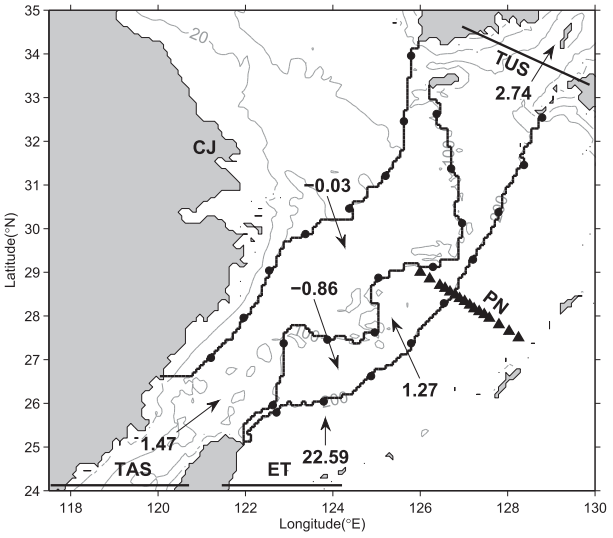

FIG. 1. Model bathymetry in the ECS. Regions are designated as follows: Taiwan Strait (TAS), east of Taiwan (ET), Tsushima Strait (TSU), Changjiang (CJ), and PN line (PN). Triangles represent observation points along the PN line. Contour lines in gray represent the real 20-, 50-, 100-, and 200-m isobaths. Contour lines in black represent the 50-, 100-, and 200-m isobaths designated in this study. Between each set of adjacent black dots on the black lines, there are 20 grid points. The grid points are counted from south to north. Arrows across the black contour lines represent volume transport across the contour with the indicated magnitude (Sv).

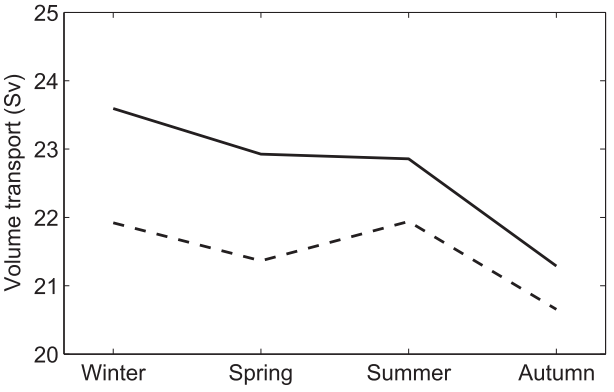

FIG. 2. Seasonal variation of geostrophic volume transport across the PN line. The solid line is averaged from the values for each season in Wei et al. (2013); the dashed line is from the reanalysis data of JCOPE2. The period of average for the two lines is from 1993 to 2009.

September to November, and winter from December to February.

The inflow volume transport (IVT), outflow volume transport (OVT) and net volume transport (NVT) were calculated as follows:

$$\mathrm{IVT} = \iint u_{+}(x,z)\,dx\,dz, \tag{1}$$

$$\mathrm{OVT} = \iint u_{-}(x,z)\,dx\,dz, \quad \text{and} \tag{2}$$

$$\mathrm{NVT} = \iint u(x,z)\,dx\,dz. \tag{3}$$

Here, $u(x, z)$ is the daily velocity component normal to the isobath, while subscripts + and − denote the directions of onshore and offshore, respectively. The term x is the horizontal coordinate along the isobaths, and dx is the horizontal interval of grid points. The term z is the vertical coordinate and dz is the vertical interval of grid points.

We compared the reanalysis data with observations at the PN line (see Fig. 1 for its position), where long-term routine hydrographic measurements were carried out by the Japan Meteorological Agency. The volume transport across the PN line was often referred to as the Kuroshio volume transport in the ECS (Ichikawa and Beardsley 2002). Using observed hydrographic data for the years from 1955 to 2010 and the inverse method, Wei et al. (2013) provided quarterly geostrophic volume transport across the PN line. The mean geostrophic volume transport averaged from 1993 to 2009 [we discard 2010 because there is only a value for winter of 2010 in Wei et al. (2013)] was 22.67 Sv with a maximum in winter (23.59 Sv) and a minimum in autumn (21.29 Sv; Fig. 2).

For comparison, we calculated the quarterly geostrophic velocity along the PN line using the density from JCOPE2 reanalysis data at the same locations as the observation and assuming a level of no motion at 700-m depth. The mean geostrophic volume transport across the PN line was estimated to be 21.47 Sv, which was a little smaller than the observed value of 22.67 Sv (Fig. 2). The difference in two mean transports is likely attributed to the difference of dynamic method we used and the inverse method Wei et al. (2013) used. As demonstrated by Wei et al. (2013), the geostrophic volume transport at the PN line calculated by the dynamic method was usually smaller than that by the inverse method by about 1 Sv.

The geostrophic volume transport obtained from the reanalysis showed a similar seasonal variation as the observation: maximum in winter and minimum in autumn (Fig. 2). The transport from the reanalysis in summer was comparable with that in winter, which is a little different from that in the observations where the transport is slightly smaller in summer than in winter. Considering the uncertainty of seasonal variations in the transport from observations (four times a year) at the PN line, the slight difference in summer is probably acceptable. Soeyanto et al. (2014) also made a

comparison of the volume transport through the PN line between Wei et al. (2013) and the JCOPE2 reanalysis data but for the interannual variations and reported a significant correlation between the two data sources. Therefore, we consider that the JCOPE2 reanalysis well represents the seasonal and interannual variations of the Kuroshio in the ECS.

3. Analysis results

We divided our analysis into two parts: mean state and temporal (mainly seasonal) variation. The mean state results were averaged over the entire 20-yr reanalysis period. The seasonal variations were examined from monthly means over 20 yr for the same month.

a. Mean state of currents across isobaths

1) MEAN VOLUME TRANSPORTS ACROSS ISOBATHS

The mean volume transports across the three isobaths in the ECS differed greatly (Fig. 1). The NVT across the 200-m isobath (1.27 Sv in the direction from the Kuroshio to outer shelf) agrees well with the previous observations [3 Sv averaged from October to December in Teague et al. (2003); 1.4 Sv in Isobe (2008)] and model results [e.g., 1.46 Sv in Guo et al. (2006); 1.17 Sv in Zhou et al. (2015)]. The IVT and OVT across the 200-m isobath of 31.82 and −30.55 Sv, respectively, are consistent with the results from a different model (29.06 and −27.70 Sv in Zhao and Guo 2011) and much larger than the corresponding NVT. The NVT across the 100-m isobath was −0.86 Sv, indicating movement in an offshore direction from midshelf to outer shelf. The IVT (5.30 Sv) and OVT (−6.16 Sv) across the 100-m isobath are much larger than the NVT (−0.86 Sv). The 50-m isobath and coastal line round up a closed area, into which the Changjiang is the only source of water. The annual-mean discharge from the Changjiang is approximately 0.03 Sv (averaged over 1993 to 2012). Consequently, we obtained a very small NVT across the 50-m isobath (−0.03 Sv). The IVT and OVT across the 50-m isobaths were 1.98 and −2.01 Sv, respectively, which are both larger than the NVT.

The mean volume transport through the Taiwan Strait was 1.47 Sv in the JCOPE2 reanalysis (Fig. 1). From the perspective of the water budget in the ECS, water from the Taiwan Strait has two exits. About 60% goes across the 100-m isobath into the outer shelf and contributes 0.86 Sv to the NVT of the 100-m isobath. The other 40% goes through the Jeju Strait and then heads to the Tsushima Strait. The offshore shelf water across the 100-m isobath (0.86 Sv) and the onshore Kuroshio water across the 200-m isobath (1.27 Sv) come together in the outer shelf and exit the ECS from east of Jeju toward the Tsushima Strait.

2) HORIZONTAL DISTRIBUTION OF THE MEAN CURRENTS ACROSS THE ISOBATHS

Taking a closer look at the cross-isobath volume transport over the continental shelf (Fig. 1), we examined the spatial distribution of the cross-isobath currents. The mean currents at the depth of 5 m, the middle of the depth, and 10 m above the sea bottom are shown in Fig. 3.

Many characteristic currents such as Kuroshio Branch Current, Taiwan Strait Current, and the China Coastal Current can be identified in the distribution of currents at the depth of 5 m (Fig. 3a). The KBCNT intrudes onshore and soon returns to the Kuroshio main stream, which is responsible for the pair of onshore and offshore currents off the northeast of Taiwan Island as denoted by the red and blue thick lines along the 200-m isobath (Fig. 3a). The Kuroshio main stream flows northeastward along the 200-m isobath before reaching the area around 30°N where it turns to the east and leaves the ECS. The KBCWK appears around 30°N and flows toward the Tsushima Strait (Fig. 3a). The Taiwan Strait Current flows northeastward from the Taiwan Strait toward 28°N, 122.7°E and splits into two branches: the offshore branch flows northeastward through the ladder-shaped, the 100-m isobath south of 29.3°N, resulting in the surface current alternatively changing directions (onshore or offshore); the onshore branch of the Taiwan Strait Current goes straight to the south of Changjiang estuary at about 29.5°N, where a small portion of it intrudes across the 50-m isobath between grid points 75 and 95, but it soon turns eastward. In the coastal region south of the Changjiang estuary, the coastal currents flow southward and cross the 50-m isobath offshore.

Currents at 10 m above the sea bottom are almost oriented in an onshore direction (black arrows in Fig. 3b), especially in the areas northeast of Taiwan, the middle of the shelf break, and southwest of Kyushu. In the area northeast of Taiwan (25°–28°N, 122°–123°E), the onshore bottom current becomes apparent between the 100- and 200-m isobaths and flows northward across the 50-m isobath to the offshore Changjiang area; in the middle area of the shelf break (27°–29°N, 125°–126°E), the bottom current flows northward from the 200- to 100-m isobaths and continues northward along the 100-m isobath to the west of Jeju Island where it turns northwestward across the 50-m isobath; in the area southwest of Kyushu (30°–33°N, 127°–128°E), the bottom current flows northwestward

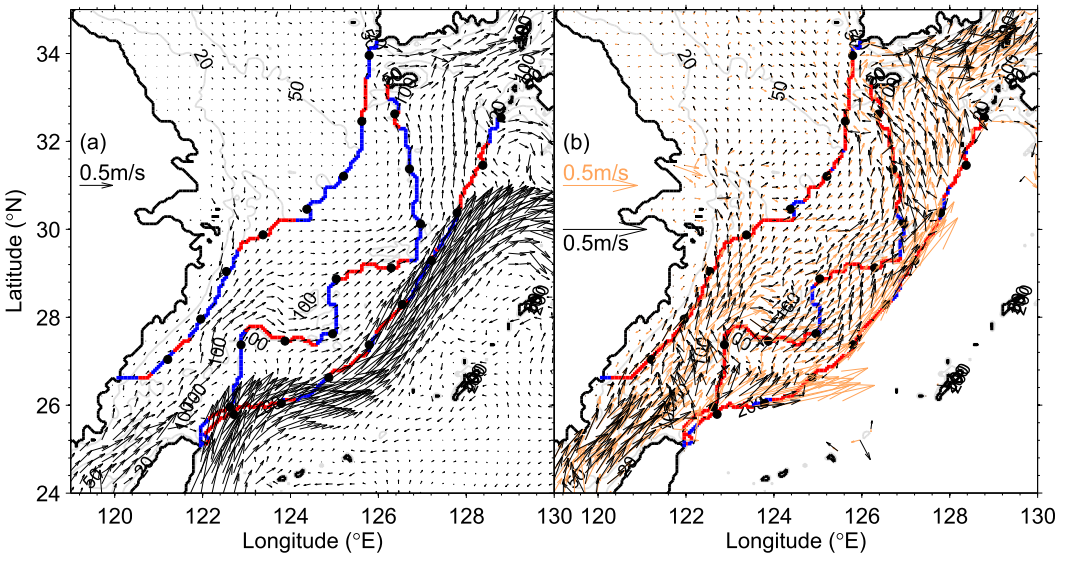

FIG. 3. Annual-mean current distribution (a) at depth of 5 m, and (b) at middepth (brown arrows) and at 10 m above the sea bottom (black arrows). Current in the areas deeper than 300 m is not shown in (b). Red (blue) thick lines along the isobaths indicate the presence of an onshore (offshore) current component.

between the 100- and 200-m isobaths and turns northeastward to the Tsushima Strait.

The Taiwan Strait Current in the bottom (Fig. 3b) likely bifurcates as it does in the surface (Fig. 3a). The onshore branch flows close to the coast and intrudes onshore across the 50-m isobath up to 30°N. The offshore branch heads northeastward and goes offshore across the 100-m isobath at 28° and at 30°N, respectively, and goes onshore between them. Consequently, the cross-isobath current at the bottom demonstrates an

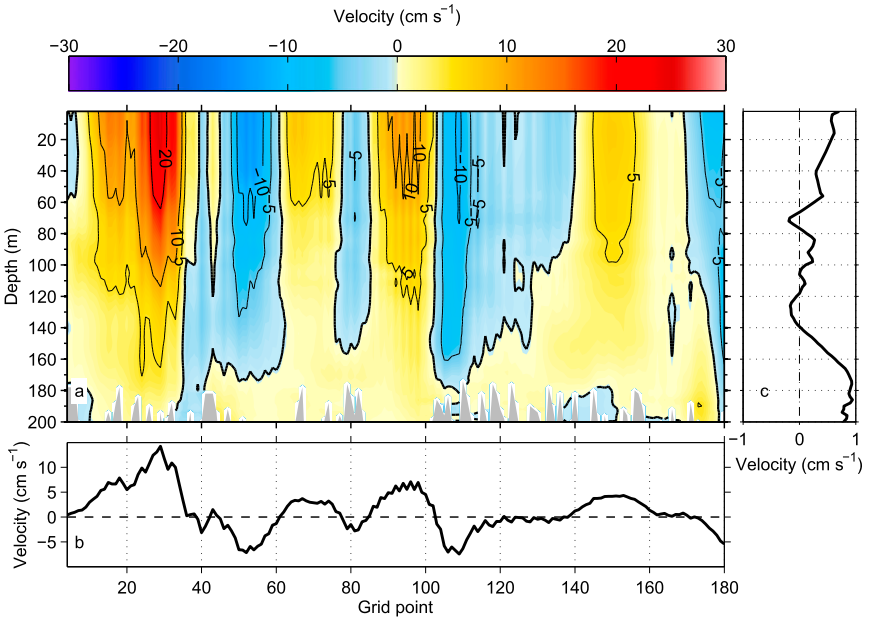

FIG. 4. (a) Vertical distribution of the current component across the 200-m isobath for the annual-mean flow field. (b) Vertical average of the current component in (a). The *x* axis shows the grid points along the 200-m isobath starting from the south end (Fig. 1). (c) Horizontal average of the current component in (a). Positive (negative) values indicate the current component is flowing in an onshore (offshore) direction.

alternation in the current direction of onshore and offshore along the 100-m isobath.

3) VERTICAL DISTRIBUTION OF THE MEAN CURRENTS ACROSS THE ISOBATHS

Along the 200-m isobath for which the gridpoint numbers are given as the horizontal coordinates, the cross-isobath currents show a stripelike distribution, indicating that the variation of velocity is smaller in the vertical direction than in the horizontal direction (Fig. 4a). Based on direction, the cross-isobath velocities can be divided into several water columns along the 200-m isobath. The velocities are in the onshore direction from the sea surface to bottom in some water columns (grid points 5–36, 60–78, 85–103, and 150–170) but are in the offshore direction from the sea surface to a depth of ~160 m and in the onshore direction from ~160 m to the sea bottom in the other columns (grid points 45–60, 78–85, and 103–130). The onshore and offshore velocities are largest at the surface of grid points 30 and 52, respectively. The maximum onshore velocity (25 cm s^{-1}) is larger than the offshore one (13 cm s^{-1}). Both the largest onshore and offshore velocities appear northeast of Taiwan, where the KBCNT intrudes onto the shelf, and some of it returns back to the shelf break, forming the pair of strong onshore velocity and less strong offshore velocity at grid points 30 and 52, respectively.

The vertical average of cross-isobath velocities suggests that there are three main onshore intrusion locations: northeast of Taiwan (grid points 1–40), middle of the shelf break (grid points 85–100), and southwest of Kyushu (grid points 140–170; Fig. 4b). All have been reported in previous studies (Guo et al. 2006; Liu et al. 2014; Zhou et al. 2015). In general, the vertically averaged cross-isobath velocity along the 200-m isobath has a magnitude less than 5 cm s^{-1}. The largest is 14 cm s^{-1}, appearing northeast of Taiwan in an onshore direction.

The horizontal average of the cross-isobath velocities can be divided into three layers according to flow direction (Fig. 4c): surface layer (0–60 m), midlayer (60–140 m), and bottom layer (140–200 m). In the surface layer, the direction is onshore with a magnitude between 0.5 to 1.0 cm s^{-1}; in the midlayer, the direction is unstable with a magnitude less than 0.5 cm s^{-1}; and in the bottom layer, the direction is onshore, which is the same as for the surface layer but with a slightly larger magnitude (close to 1.0 cm s^{-1}). In the surface layer, the cross-isobath velocity at each grid point is strong but the direction changes frequently along the isobath (Fig. 4a), resulting in a small, horizontal, averaged flow (Fig. 4c). In the bottom layer, the cross-isobath velocity at each grid point is almost in the onshore direction, and the cancellation of positive and negative velocities does not occur during horizontal averaging, producing a stronger, horizontally averaged, cross-isobath velocity in the bottom layer than in the surface layer (Fig. 4c).

The cross-isobath velocities along the 100-m isobath (Fig. 5a) show the same stripelike distribution as those along the 200-m isobath but with smaller magnitudes (<10 cm s^{-1}) than those along the 200-m isobath. The onshore currents appear mainly at grid points 1–20, 42–75, and 100–128. At grid points 1–20 and 42–75, the velocities reach maxima (~7 cm s^{-1}) in the bottom layer, which is different from the case along the 200-m isobath, where the largest onshore velocity appears in the surface layer. At grid points 100–128, the velocities are in an onshore direction from the surface to the bottom with little change. The offshore cross-isobath velocities along the 100-m isobath are mainly in the surface layers at grid points 20–40, 75–100, and 128–173 where onshore cross-isobath velocities are still evident in the bottom layer at grid points 20–40 and 128–173.

Taking the vertically averaged cross-isobath velocities for the 100-m isobath (Fig. 5b), the maximum offshore velocity is larger than the onshore one, and there are more areas where the velocities are in the offshore direction than in the onshore direction. The horizontally averaged velocities show a two-layer structure: offshore in the surface layer (0–80 m) and onshore in the bottom layer (80–100 m; Fig. 5c). In the upper 80-m layer, the magnitude changes little with depth. However, the velocities are in the opposite direction in the bottom layer with a maximum velocity over 2.5 cm s^{-1}, which is larger than that at the 200-m isobath (Fig. 4c). The thickness of the bottom onshore velocity layer at the 100-m isobath (20 m: 80–100-m depth) is thinner than that at the 200-m isobath (60 m: 140–200-m depth).

For the 50-m isobath, except for at the ends, the magnitude of the velocity is under 3 cm s^{-1}, which is weaker than the other two isobaths, but the stripe-type distribution is maintained (Fig. 6a). The cross-isobath velocities change little in the vertical direction at some positions (grid points 22–30, 70–92, and 140–152) but show a two-layer vertical structure at other positions (grid points 30–70 and 95–140) where the cross-isobath current flows shoreward from a depth of 35 m to the sea bottom. The largest onshore and offshore velocities appear at two ends of the 50-m isobath, where the Taiwan Strait Current and the West Korea Coastal Current, respectively, flow and result in the large cross-isobath velocities.

The vertically averaged cross-isobath current along the 50-m isobath is in the onshore direction at grid points 65–92 and 136–154 with a magnitude around 3.0 cm s^{-1} and is in the offshore direction at some other grid points

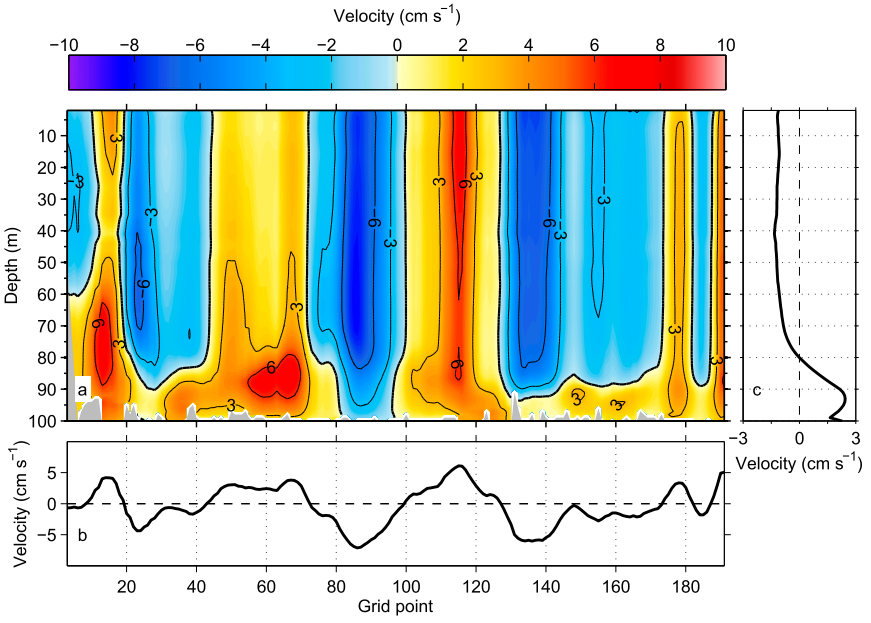

FIG. 5. As in Fig. 4, but for the 100-m isobath.

(Fig. 6b). The horizontally averaged cross-isobath current along the 50-m isobath presents an apparent two-layer structure (Fig. 6c): in the offshore direction from 0- to 34-m depth with a maximum speed of 1.7 cm s^{-1} at the surface and in the onshore direction from 34 m to the bottom with a velocity close to 1.0 cm s^{-1}.

To obtain a general idea of the water exchange over the continental shelf in the ECS, we make a comparison of the horizontally averaged cross-isobath velocities at the three isobaths. The horizontally averaged cross-isobath velocities show a two-layer structure at the 50- and 100-m isobaths (onshore in the bottom layer but offshore in the upper layer) and a three-layer structure at the 200-m isobath (onshore in both the surface and bottom layers but unstable in the midlayer). The common feature among the three isobaths is that the velocity

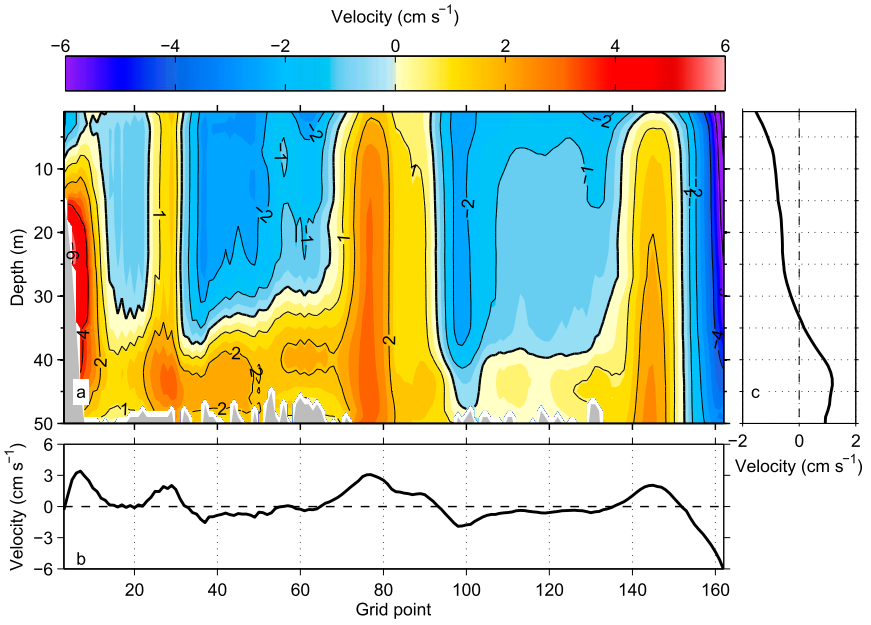

FIG. 6. As in Fig. 4, but for the 50-m isobath.

is in the onshore direction in the bottom layer. The thickness of the onshore bottom layer is 60, 20, and 16 m at the 200-, 100- and 50-m isobaths, respectively; the maximum onshore velocity is approximately 1, 2.5, and 1 cm s^{-1} at the 200-, 100-, and 50-m isobaths, respectively. As shown in Fig. 3b, the bottom currents veer left against the currents in the middepth. This feature of the bottom Ekman dynamics has been recognized in the current mooring data (Hu 1994; Yoshikawa et al. 2010) and in the numerical model results (Jacobs et al. 2000; Guo et al. 2006).

b. Seasonal variations of currents across isobaths

1) Seasonal variations of IVT, OVT, and NVT across isobaths

The IVT across the 200-m isobath has a maximum in November (32.90 Sv), while the OVT peaks at 31.50 Sv in April (Fig. 7a). Both IVT and OVT across the 200-m isobath are lowest in December and January with a minimum value of 30.50 and 29.20 Sv, respectively. Although the IVT and OVT show similarly weak seasonal patterns, the difference (NVT) shows significant seasonal variation. The NVT across the 200-m isobath is positive throughout the year but is highest in October (1.90 Sv) and lowest in April (0.75 Sv).

The IVT across the 100-m isobath has a maximum of 5.73 Sv in April and a minimum of 5.04 Sv in July (Fig. 7b). The OVT across the 100-m isobath reaches a maximum of 6.86 Sv in April and a minimum of 5.50 Sv in October. The range of seasonal variation is smaller for the IVT than for the OVT, and the NVT is negative throughout the year across the 100-m isobath. The NVT is in the offshore direction and the strongest (−1.39 Sv) and weakest (−0.29 Sv) values are in summer and autumn, respectively.

The IVT and OVT across the 50-m isobath maintain a balance throughout the year. The maxima (~2.87 Sv) and minima (~1.35 Sv) appear in summer and winter, respectively (Fig. 7c). The NVT across the 50-m isobath is largest in October and smallest in January.

2) Seasonal variations of horizontally averaged cross-isobath currents

The horizontal averages of the cross-isobath currents (Figs. 4c, 5c, and 6c) show a clear two-layer or three-layer structure. Their seasonal variations are also important to our analysis from the viewpoint of water exchange between the shelf and the Kuroshio region.

The horizontal average of currents across the 200-m isobath is divided into three layers according to the direction of flow: surface layer (0–60 m) and bottom layer (140 m–bottom) have an onshore direction, and the

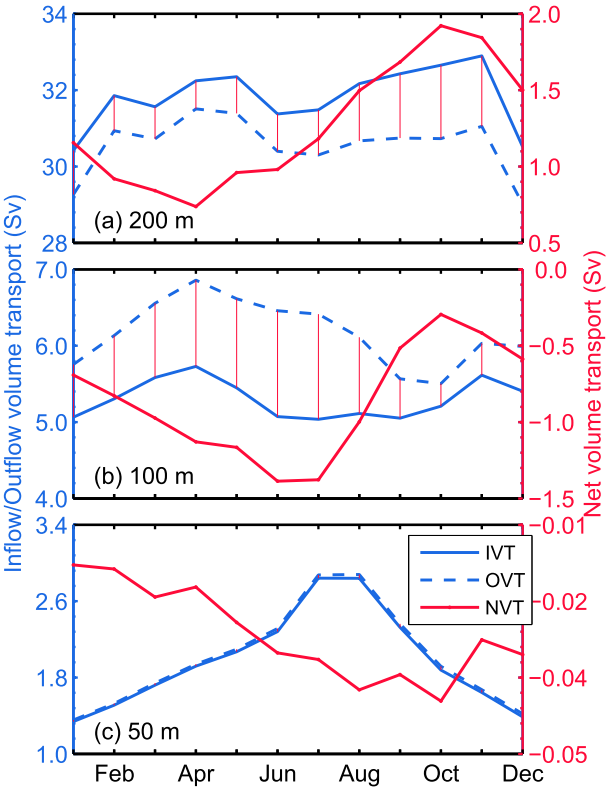

FIG. 7. Monthly volume transport of IVT (solid blue), OVT (dashed blue), and NVT (red) across the (a) 200-, (b) 100-, and (c) 50-m isobaths. The OVT is by definition a negative value, but for easy comparison with IVT, we present the absolute value of OVT. The red bar indicates the difference between IVT and OVT, namely, NVT.

midlayer (60–140 m) has an unstable direction (Fig. 4c). The horizontally averaged currents in these three layers have diverse seasonal variations (Fig. 8a). In the surface layer, the horizontal average of cross-isobath currents is in the onshore direction in autumn and winter and in the offshore direction in summer (from May to August). In the midlayer, the horizontal average of cross-isobath currents is in the onshore direction in summer and in the offshore direction in winter. In the bottom layer, the horizontally averaged currents are always in the onshore direction with a weak seasonality as shown by contours in Fig. 8a. Apparently, the seasonal variations occur mainly in the surface and midlayers. The seasonal variations in these two layers are generally opposite, especially in summer and winter, and the pattern in the surface layer precedes that in the midlayer by about 1–2 months.

Both the horizontal averages of currents across the 100- and 50-m isobaths show a two-layer structure (Figs. 5c, 6c): offshore in the surface layer and onshore in the bottom layer. At the 100-m isobath (Fig. 8b), except

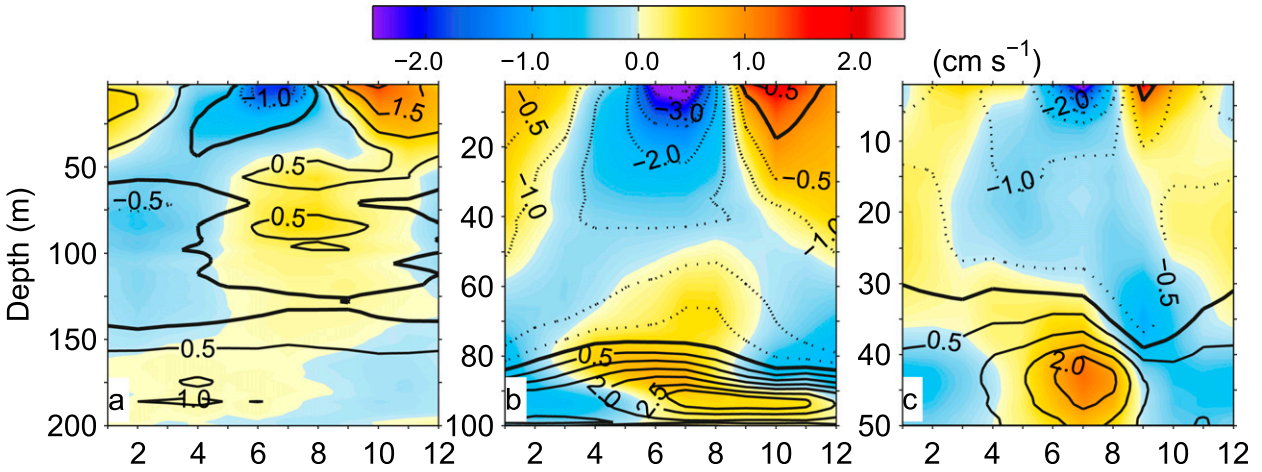

FIG. 8. Monthly mean (contours) and anomaly (colors) of the horizontally averaged currents across the (a) 200-, (b) 100-, and (c) 50-m isobaths. The solid (dashed) contours indicate currents are in the onshore (offshore) direction; thick black lines denote zero value. The anomaly is the monthly mean of the horizontally averaged currents across the isobath minus the annual-mean one. The negative anomaly of offshore current means that the offshore current is stronger than the mean offshore one.

for the upper 20-m layer in autumn, the horizontal average of the cross-isobath currents in the surface layer (0–80 m) is in the offshore direction, and the maximum offshore velocity occurs in summer; that in the bottom layer (80–100 m) is in the onshore direction throughout the year and peaks at about 2.9 cm s^{-1} in summer. At the 50-m isobath (Fig. 8c), the horizontal average of the cross-isobath currents in the surface layer (0–34 m) is always in the offshore direction except for in the upper 5 m in September and reaches its maximum in summer; that in the bottom layer (34–50 m) is in the onshore direction throughout the year and reaches its maximum in summer. Therefore, the two-layer structure at the 100- and 50-m isobaths shows the same seasonal variation: strong in summer and weak in winter.

The volume transport of the cross-isobath current in each layer of the two- or three-layer structure at the three isobaths presents a quantitative view to this issue (Fig. 9). At the 200-m isobath, the mean NVT in the midlayer is very small (0.1 Sv), which is only a quarter of the NVT in the surface layer (0.38 Sv) and an eighth of the NVT in the bottom layer (0.79 Sv; Fig. 9a). The seasonal variations of the NVT in the surface and midlayers at the 200-m isobath are apparent, but the pattern is the opposite with similar amplitude (standard deviation of 0.41 Sv in the surface layer and 0.31 Sv in the midlayer). From a viewpoint of the intensity of onshore intrusion, the NVT in the surface layer of the 200-m isobath is minimum in summer and maximum in autumn and winter, while that in the midlayer is maximum in summer and minimum in winter. The seasonality of NVT in the bottom layer is weak with a standard deviation of only 0.04 Sv, which is one order of magnitude smaller than those in the surface and midlayers.

At the 100-m isobath (Fig. 9b), the mean NVT is 1.42 Sv offshore in the surface layer and 0.55 Sv onshore in the bottom layer. The seasonal variation of NVT across the 100-m isobath occurs mainly in the surface layer where the offshore NVT is strongest in summer (>2 Sv) and weakest in winter (~1 Sv). The seasonal variation of NVT across the 100-m isobath in the bottom layer is much weaker than that in the surface layer but it still exists; it increases from February to July and then decreases gradually until reaching its minimum in January.

At the 50-m isobath (Fig. 9c), the mean NVT is −0.34 Sv offshore in the surface layer and 0.31 Sv onshore in the bottom layer. The seasonal fluctuation in the two layers shows almost the same pattern.

In this study, we do not give details on the interannual variation of cross-isobath currents but report this variation in the context of a comparison with seasonal variation. The bars in Fig. 9 indicate the standard deviation of the interannual variation for each month. The interannual variations of NVTs in all layers of the three isobaths, except for the bottom layer of the 200-m isobath, are generally weaker than the corresponding seasonal variations and the range of interannual variations is 50%–60% of the seasonal ranges. Therefore, the water exchange over the shelf in the direction of the cross-isobath flow is dominated by seasonal variation, and interannual variation does not qualitatively change the pattern we report here for seasonal variation.

4. Mechanisms

In section 3, we showed the vertical structures and seasonal variations of currents in different layers across

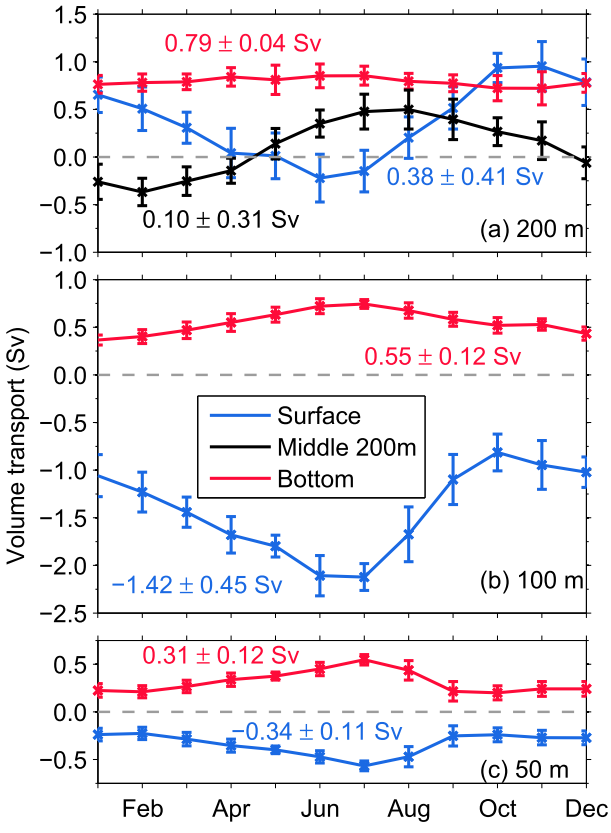

FIG. 9. Seasonal variation of NVT in (a) three layers of the 200-m isobath and two layers of the (b) 100- and (c) 50-m isobaths. Blue lines denote the NVT in the surface layer; red lines denote the NVT in the bottom layer; and black line denotes the NVT in the midlayer of the 200-m isobath. The depth ranges of surface, mid-, and bottom layer of the 200-m isobath are 0–60, 60–140, and 140–200 m, respectively. The depth ranges of surface and bottom layers of the 100-m isobath are 0–80 and 80–100 m. The depth ranges of surface and bottom layers of the 50-m isobath are 0–34 and 34–50 m. The annual mean plus or minus standard deviation (Sv) are given next to the line. The bar inside the line denotes the standard deviation of interannual variation in each month calculated from the anomaly in the same month during a period of 1993 to 2012.

the three isobaths. Next, we examine mechanisms that likely control the seasonal variations of NVTs in those layers.

a. Surface layer of all three isobaths

The surface layer of the 200-m isobath ranges in depth from 0 to 60 m and has an NVT in the onshore direction in autumn and winter and in the offshore direction in summer, showing the most prominent seasonal variation among the three layers of the 200-m isobath. This result is consistent with the report by Guo et al. (2006). Guo et al. (2006) proposed that the wind-induced Ekman transport accounts for the seasonal variation of NVT in the surface layer of the 200-m isobath. Following this idea, we calculated the Ekman transport VT_S as follows with $VT_S = \int \tau_s/(\rho_0 f)\, dx$, where τ_s is wind stress in the direction along the isobath, ρ_0 is water density, f is the Coriolis parameter, and dx is the horizontal interval of the grid points along the isobath. Surface Ekman transport across the three isobaths shows similar seasonal variations with a weak offshore transport in summer and strong onshore transport in winter (Fig. 10).

Surface Ekman transport across the 200-m isobath (red line in Fig. 10) agrees well with the NVT in the surface layer of the 200-m isobath (blue line in Fig. 9a). Both reach a minimum in June at about −0.24 Sv and a maximum in November at 0.95 Sv for NVT and in December at 1.04 Sv for the Ekman transport. The slight difference between the values of these two in winter indicates the possible presence of other mechanisms. However, the local wind is likely the major factor controlling the seasonal variation of the NVT in the surface layer of the 200-m isobath.

It is needed to emphasize that the NVT in the surface layer of the 200-m isobath is the total volume transport integrated over the entire shelf break. Both Oey et al. (2010) and Wu et al. (2014) proposed that in winter the local wind is not responsible for the Kuroshio intrusion northeast of Taiwan. From the observations, Tang and Yang (1993) and Chuang and Liang (1994) found that the currents northeast of Taiwan were not well correlated with the local wind; onshore intrusion of Kuroshio water occurred 1 month after the starting of the northeast monsoonal wind during the fall to winter season. This conclusion is also true in our reanalysis data. If we calculated the onshore volume transport across the 200-m isobath only northeast of Taiwan, we also need a 1-month lag to obtain a good correlation between the Ekman transport and the onshore transport (figures not shown here). It is only the surface transport across the entire 200-m isobath from northeast of Taiwan to southwest of Kyushu that shows a good correlation with the corresponding surface Ekman transport without a time lag.

Regarding the above difference between northeast of Taiwan and the entire shelf break, Guo et al. (2006) demonstrated that for the Kuroshio onshore flux across the entire shelf break, its seasonal variation was primarily controlled by the Ekman transport while the change in the density field was secondary. For the Kuroshio onshore flux at a fixed location along the shelf break, its seasonal variation was primarily related to the change in density field and the Ekman transport was secondary. Zhou et al. (2015) also indicated that the Ekman effects to some extent are responsible for variability in the upper-layer exchanges. Therefore, our results from the JCOPE reanalysis data are consistent with the previous studies.

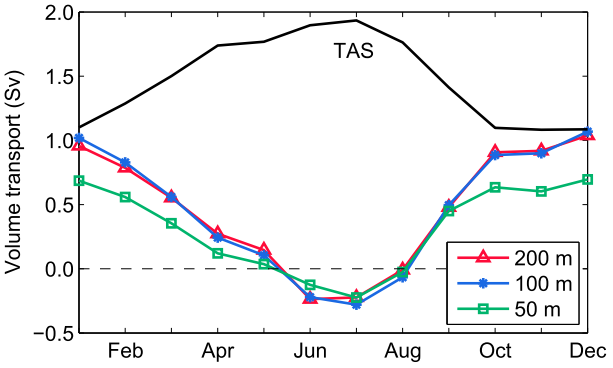

FIG. 10. Monthly volume transport through the Taiwan Strait (TAS; black line) and surface Ekman transport across the 200- (red), 100- (blue), and 50-m (green) isobaths.

Similarly, surface Ekman dynamics can also be applied to the cross-isobath current at the 100- and 50-m isobaths. However, wind-driven Ekman transport alone cannot explain the NVT across the 100- and 50-m isobaths. The horizontally averaged cross-isobath currents in the surface layer of the 100- and 50-m isobaths are in the offshore direction throughout the year (blue lines in Figs. 9b and 9c), which contrasts with onshore surface Ekman transport in autumn, winter, and spring (blue and green lines in Fig. 10).

The horizontal distribution of currents at a depth of 5 m in January and July suggests that the Taiwan Strait water is the main source of the offshore NVT in the surface layer of the 100-m isobath (Fig. 11). In July, the volume transport of the Taiwan Strait Current becomes large (black line in Fig. 10), and the currents across the 100-m isobath also become strong, especially at about 28°N and south of Jeju Island (Fig. 11). At this moment, the NVT in the surface layer of the 100-m isobath (0–80 m) is about 2 Sv (Fig. 9b), which is comparable to the volume transport through the Taiwan Strait (1.90 Sv; black line in Fig. 10). Both of them become weak in autumn and winter (about 1 Sv). Since the surface Ekman transport across the 100-m isobath in July is only −0.28 Sv, it cannot even explain the NVT in the upper 20 m of the 100-m isobath (−0.90 Sv). Therefore, the Taiwan Strait Current must be the major controlling factor for the seasonal variations of NVT in the surface layer of the 100-m isobath.

The main factor determining the NVT in the surface layer of the 50-m isobath is likely from the Changjiang (Fig. 11). Since the annual mean of the Changjiang discharge is 0.03 Sv, which is one order smaller than the NVT in the surface layer of the 50-m isobath, the river water itself contributes little to the NVT in the surface layer of the 50-m isobath. However, the buoyancy effect from the Changjiang water is an important driving force of circulation in the ECS (Naimie et al. 2001). The increase of river discharge results in the increase of buoyancy, and more shelf water moves seaward from the surface layer, which should be compensated by bottom landward flow. In general, the density-driven current in an estuary region is larger than the river discharge by about one order of magnitude (Dyer 1979; MacCready and Geyer 2010). It follows that the NVT in the surface layer (0.34 Sv) and the bottom layer (0.31 Sv) of the 50-m isobath can theoretically result from the buoyancy effect of Changjiang water.

Changjiang discharge is high in summer and low in winter. This is similar to the NVT in the surface layer of

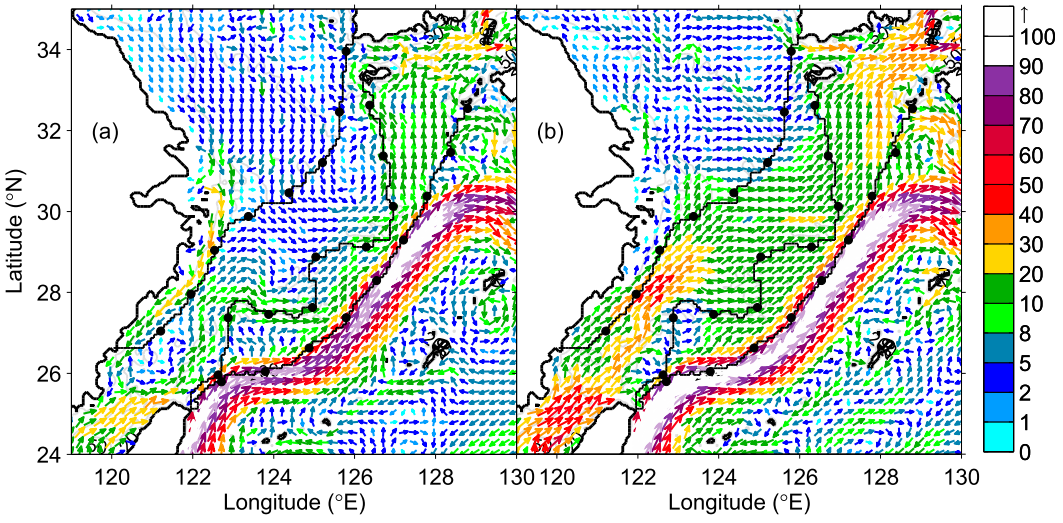

FIG. 11. Mean current distribution at 5-m depth in (a) January and (b) July. The arrows denote the current direction and the color denotes the velocity magnitude (cm s^{-1}).

the 50-m isobath (Fig. 9c). The surface Ekman transport across the 50-m isobath in summer is in the offshore direction at about 0.3 Sv (Fig. 10). But in reality, this value should be smaller than 0.3 Sv because of the limited water depth. Therefore, the strongest offshore NVT in the surface layer of the 50-m isobath in summer (about 0.5 Sv) is probably the result of a combination of the wind and Changjiang water (e.g., Chang and Isobe 2003). In winter, the surface Ekman transport across the 50-m isobath is in the onshore direction but the NVT in the surface layer of the 50-m isobath remains in the offshore direction. A possible reason for this difference is that the southward current from the Changjiang mouth along China coast in winter contributes to the offshore transport across the 50-m isobath (Fig. 11a). This southward current has been observed recently by Wu et al. (2013).

b. *Midlayer of the 200-m isobath*

The NVT in the midlayer of the 200-m isobath shows prominent seasonal variation despite that the midlayer is away from the surface layer (black line in Fig. 9a). The NVT in the midlayer of the 200-m isobath is in the onshore direction in summer and autumn and in the offshore direction in winter and spring, which is opposite to that of the surface layer. Therefore, it is difficult to associate the wind with the seasonal variation of the NVT in the midlayer of the 200-m isobath.

The monthly anomaly of Coriolis force in the along-isobath direction due to the cross-isobath current shows almost the same seasonal variation as the monthly anomaly of the pressure gradient in the along-isobath direction (Fig. 12). Apparently, the seasonal variation in the current across the 200-m isobath at the midlayer is generally in a geostrophic balance. Many previous studies have examined the vertically integrated currents across the shelf slope of ECS using a concept of joint effect of baroclinicity and relief (JEBAR; Guo et al. 2003, 2006; Oey et al. 2010; Liu et al. 2014; Wang and Oey 2016). Theoretically, the balance between the JEBAR and advection of the geostrophic potential along an isobath is equivalent to a geostrophic balance in the direction along the isobath (Oey et al. 2010). Since the midlayer (60–140-m depth) of the 200-m isobath is beyond the control of surface and bottom boundary layers, the dominant role of geostrophic currents there is likely reasonable (Zhou et al. 2015; Ding et al. 2016).

To illustrate the seasonal variation of the density gradient along the isobath, we show the vertical distribution of water temperature along the 200-m isobath in winter (February) and summer (August) in Fig. 13. Because of the weak contribution of the salinity difference, the distribution of the water temperature along the

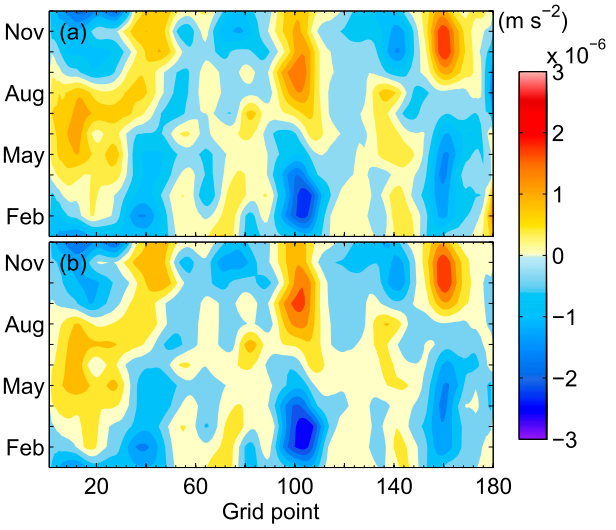

FIG. 12. Monthly anomaly (difference of monthly mean from the annual mean) of (a) the along-isobath Coriolis force and (b) the along-isobath pressure gradient force. The anomalies are vertically averaged from 60- to 140-m depth along the 200-m isobath. A positive anomaly means intensification of an onshore flow or weakening of an offshore flow. The abscissa is the grid number along the 200-m isobath starting from northeast of Taiwan and ending southwest of Kyushu.

200-m isobath is similar to that of the density. As an example of geostrophic balance, we focus on the area around grid point 105, the location with the most prominent seasonal variation. According to Fig. 4a, the cross-isobath currents in the midlayer of the 200-m isobath are onshore (offshore) at the left (right) side of grid point 105. This feature is consistent with the spatial variation of water temperature whose isotherms steepen northward (southward) on the left (right) side of grid point 105. In summer, the stratification is intensified and the isotherms become dense, indicating the increases of alongshore gradient and onshore intrusion on the left side of grid point 105. However, on its right side, the isotherms are less slanted, resulting in a smaller alongshore gradient and a weaker offshore current there in summer than in winter.

As shown by Oey et al. (2010), spatial variation in local heat flux is a possible cause for the seasonal change in density gradient along the isobaths in the ECS. In addition, the onshore and offshore shift of Kuroshio axis associated with seasonal variation in the vertical current structure of Kuroshio (Guo et al. 2003), the change in the Kuroshio current speed associated with basin-scale change in wind field and arrival of mesoscale eddies (Soeyanto et al. 2014), and the seasonal variation in the Kuroshio density structure associated with basin-scale heat flux are also expected to affect the onshore and offshore flow in the midlayer of the 200-m isobath from a

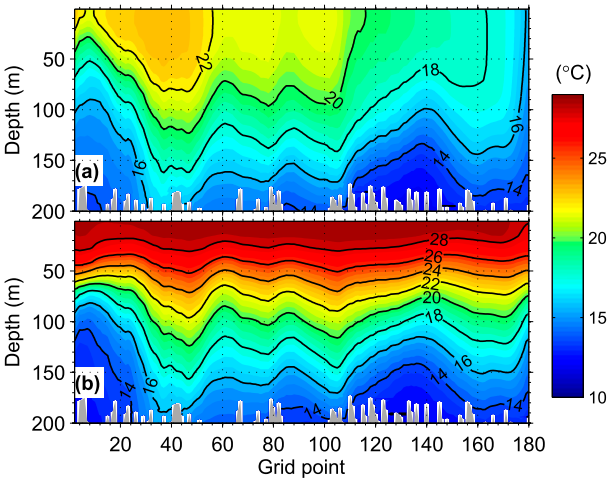

FIG. 13. Temperature distribution along the 200-m isobath in (a) February and (b) August. The grid points are counted from south to north.

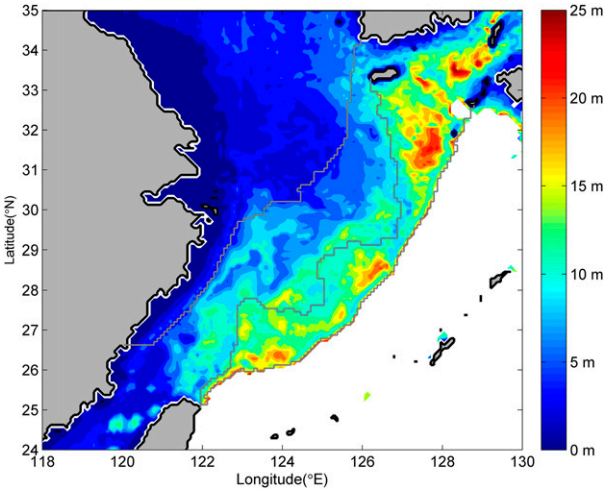

FIG. 14. Distribution of mean bottom Ekman thickness in the ECS. Bottom Ekman thickness in the areas deeper than 250-m depth is not shown.

viewpoint of geostrophic balance. To completely understand the contribution of these processes to the cross-isobath current in the ECS, a series of numerical experiments designed for isolating the contribution of each process similar to that in Oey et al. (2010) are necessary.

c. *Bottom layer of the three isobaths*

To examine the year-round onshore transport in the bottom layer of the three isobaths, we planned to investigate the effects of the bottom Ekman (Hu 1994; Jacobs et al. 2000; Yoshikawa et al. 2010) from two aspects: the bottom Ekman transport and bottom Ekman layer thickness. The bottom Ekman transport is typically calculated by $\mathrm{VT}_B = \int \tau_b/(\rho_0 f)\,dx$ and $\tau_b = \rho_0 C_d \sqrt{(u_b^2 + v_b^2)}\,u_b$, where τ_b is the component of bottom stress along the isobath, v_b is velocity across the isobath, u_b is velocity along the isobath, C_d is the bottom friction coefficient, and dx is the horizontal interval of the grid points along the isobaths. The bottom Ekman layer thickness is typically calculated by $D = \sqrt{A_v/(0.5f)}$, where A_v is vertical eddy viscosity. Since the reanalysis data of JCOPE2 provides us only daily averaged velocities, the nonlinear feature in the calculation for the bottom stresses and vertical eddy viscosity prevents us from obtaining an accurate value for the two variables. As an alternative, we estimated the bottom Ekman layer thickness through the veering rate based on the left-veering feature of the bottom Ekman currents in the Northern Hemisphere.

For stratified water over a sloping bottom, it has been reported that the veering rate of the horizontal bottom Ekman current is largest at the top of the bottom boundary layer (Weatherly and Martin 1978; Taylor and Sarkar 2008). We therefore define the bottom Ekman layer as the point where the first peak of the veering rate comes up from the bottom and set its upper limit as half of the water depth to avoid the case that there is no veering rate peak within a water column or the veering rate peak is found in the surface Ekman layer. We presented the distribution of bottom Ekman thickness over the ECS in Fig. 14. The averaged bottom Ekman thicknesses at the 200-, 100-, and 50-m isobaths are 17.9, 10.9, and 5.1 m, respectively, with a decreasing trend from the deep ocean to the shallow shelf sea.

Yoshikawa et al. (2010) estimated the vertical eddy viscosity through velocity profiles observed at two stations in the ECS. The water depths at the two stations are 128 and 53 m, respectively. The estimated vertical eddy viscosity peaked at 2–3 $\times$ 10^{-3} $\mathrm{m^2\,s^{-1}}$ at around 5 m above the sea bottom. By substituting this value into $D = \sqrt{A_v/(0.5f)}$, we obtained a bottom Ekman layer thickness of about 8 m. We also estimated the bottom Ekman layer thicknesses at the same two stations through the veering rate method that gives values of 16 and 5 m for the 128- and 53-m depth stations, respectively. Although the results from the two methods are not identical, they are very similar.

Based on the mooring velocity data at the 128-m depth station, Yoshikawa et al. (2010) estimated the onshore transport per unit area as 0.33 $\mathrm{m^2\,s^{-1}}$ for 11–16 October 2007 and 0.13 $\mathrm{m^2\,s^{-1}}$ for 19 August–17 October 2008. Since the bottom onshore cross-isobath currents distribute over the entire isobaths (Figs. 4–6), we multiplied the onshore transport per unit area reported by Yoshikawa et al. (2010) with the length of the

three isobaths (about 1600 km) and obtained a value of 0.53 or 0.21 Sv as the first-order approximation of the bottom onshore Ekman transport.

We next estimated the cross-isobath component of the total bottom Ekman transport with the following equation: $VT'_B = \int 0.5DU\,dx$ (Pedlosky 1987), where U is the geostrophic current, and D is the bottom Ekman layer thickness. The mean VT'_B at the 200-, 100- and 50-m isobaths are 0.60, 0.66, and 0.13 Sv, respectively, using the bottom Ekman layer thickness obtained by the veering rate method as D and the along-isobath current velocity above the bottom Ekman layer as U. The VT'_B of the 100-m isobath is a little larger than the NVT in the bottom layer of the 100-m isobath (0.55 Sv), while those of the 200- and 50-m isobaths are a little smaller than the corresponding NVT in the bottom layers of the 200-m isobath (0.79 Sv) and the 50-m isobath (0.32 Sv).

The above estimation suggests that the bottom Ekman effect is a very important process in the formation of NVT in the bottom layer of the 100-m isobath. At the 200-m isobath, the bottom Ekman effect explains only part of the NVT in the bottom layer. The density change along the isobath must also contribute to the NVT in the bottom layer of the 200-m isobath. At the 50-m isobath, the bottom Ekman effect explains only a small part of the NVT in its bottom layer. The response of the bottom layer along the 50-m isobath to the buoyancy effects of the Changjiang water is likely more important than the bottom Ekman effect to the NVT in the bottom layer of the 50-m isobath.

5. Discussion and conclusions

Using JCOPE2 reanalysis data, we presented the annual mean and seasonal variation in current velocity and volume transport across the 200-, 100-, and 50-m isobaths of the ECS. For all isobaths, the IVT and OVT show a larger magnitude than the corresponding NVT. The NVT across the 200-m isobath is 1.27 Sv in the onshore direction. The NVT across the 100-m isobath is −0.86 Sv in the offshore direction. When it comes to the 50-m isobath, the NVT is small but the IVT and OVT are about two orders of magnitude larger than that of the NVT. The seasonal variation of NVTs weakens from outer shelf to the inner shelf, and the IVT and OVT values roughly change in phase, except for the 100-m isobath.

Currents across the isobaths appear as stripelike vertical structures. At the 200-m isobath, the maximum cross-isobath velocity appears in the surface layer. The horizontal average of the cross-isobath is divided into three layers with onshore transport identified in the surface and bottom layers while the midlayer has an unstable current direction. At the 100- and 50-m isobaths, the maximum cross-isobath current occurs near the bottom. The horizontal average of the cross-isobath current is in the offshore direction in the surface layer and in the onshore direction in the bottom layer, representing a two-layer structure.

The NVTs in the vertical layers of the three isobaths are likely related to each other to a certain degree (Fig. 15). As a mean state (mean in Fig. 15), ~0.34-Sv water moves from the inner shelf to the midshelf in the surface layer of the 50-m isobath, and 1.42-Sv water moves from the midshelf to the outer shelf in the surface layer of the 100-m isobath; ~0.38- and 0.1-Sv water flow from the open ocean to the outer shelf in the surface and midlayer of the 200-m isobath, respectively, which are in the opposite direction of the cross-isobath current in the surface layers of the 50- and 100-m isobaths. In the bottom layers, all NVTs indicate the same onshore direction with values of 0.79, 0.55, and 0.31 Sv at the 200-, 100-, and 50-m isobaths, respectively. The mean NVTs in the bottom layers of the 100- and 50-m isobaths are 70% and 40% of that across the 200-m isobath, showing a decreasing trend from the 200- to the 50-m isobath. The relationship of the cross-isobath current in the bottom layers of three isobaths suggests that the bottom layer over the shelf is likely an important pathway for water exchange between the Kuroshio and continental shelf of the ECS.

The seasonal variations of the NVTs in the surface layers of three isobaths are all remarkable and similar (summer and winter in Fig. 15). In winter (summer), the offshore cross-isobath transports in the surface layers of the 50- and 100-m isobaths are weakened (intensified) while the onshore cross-isobath transport in the surface layer of the 200-m isobath is intensified (reversed to a weak offshore transport). In the bottom layers, the NVTs across the 100- and 50-m isobaths have more marked seasonality than that across the 200-m isobath. The NVT in the midlayer of the 200-m isobath shows nearly opposite seasonal variation to that in the surface layer of the 200-m isobath but nearly the same seasonal variation as in the bottom layer of the 50- and 100-m isobaths.

The controlling factor of seasonal variations varies for different vertical layers and for different isobaths. The surface Ekman transport contributes to the surface cross-isobath transport integrated over the three isobaths. The agreement of phase and magnitude between the NVT in the surface layer of the 200-m isobath and the surface Ekman transport suggests the dominant role of the winds there. However, the phase disagreement between the NVT in the surface layer of the 100- and 50-m isobaths and the surface Ekman transport suggests a

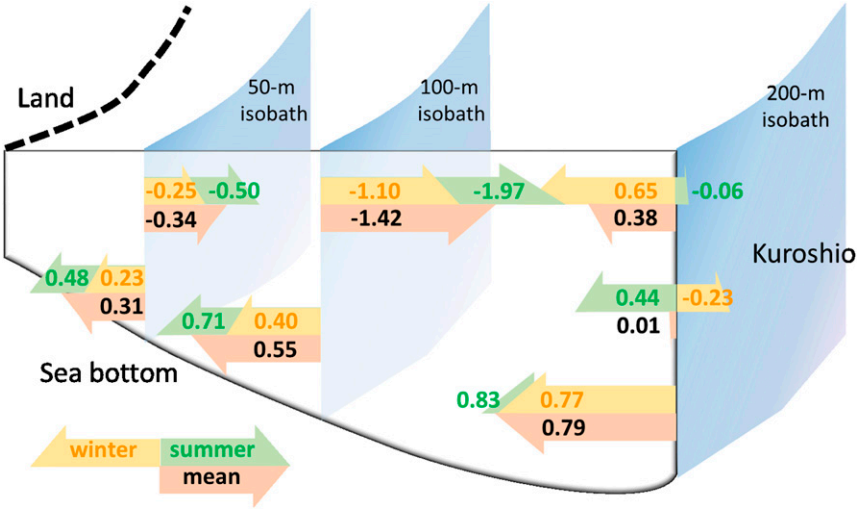

FIG. 15. Schematic diagram of water exchange across isobaths over the continental shelf of the ECS. The three isobaths are denoted by light blue sections. The horizontally averaged cross-section currents at the 50- and 100-m isobaths represent a two-layer structure and the currents at the 200-m isobath represent a three-layer structure. The depth ranges of surface, mid-, and bottom layer of the 200-m isobath are 0–60 , 60–140, and 140–200 m, respectively. The depth ranges of surface and bottom layers of the 100-m isobath are 0–80 and 80–100 m. The depth ranges of surface and bottom layers of the 50-m isobath are 0–34 and 34–50 m. The pink arrow represents the direction and magnitude of annual-mean NVT in each layer. The green and yellow arrows represent them in summer and winter respectively. Numbers near arrows denote the value of NVT (Sv).

more important contribution from other processes. The NVT in the surface layer of the 100-m isobath is likely affected more by the Taiwan Strait Current than by the surface winds and that of the 50-m isobath develops more due to the Changjiang discharge than due to the surface winds. The seasonal variation of NVT in the midlayer of the 200-m isobath is likely under a strong geostrophic balance. The bottom Ekman effect on the onshore NVT in the bottom layer is important at the 100-m isobath, partly important at the 200-m isobath, and slightly important at the 50-m isobath. The geostrophic control by the density change along the isobath also contributes to the NVT in the bottom layer of the 200-m isobath, while the response to the buoyancy effect of Changjiang discharge is important to the NVT in the bottom layer of the 50-m isobath.

The cross-shelf exchange in the ECS is a complex hydrodynamic system and is controlled by a combination of many processes. In this study, we present some mechanisms responsible for the cross-shelf currents. It is possible for us to underestimate some other mechanisms. A quantitative estimation on the contribution of each potential mechanism to the cross-shelf current needs more numerical experiments and field observations.

Acknowledgments. This study was supported by JSPS KAKENHI (26241009/26287116/H05821). J. Zhang thanks the China Scholarship Council (CSC) for supporting her stay in Japan. X. Guo thanks support from the National Natural Science Foundation of China (NSFC 41576010) and the Fundamental Research Funds for Central Universities of the Ministry of Education of China (201512004). L. Zhao thanks support from the Strategic Priority Research Program of the Chinese Academy of Sciences (XDA11020305), the NSFC (41276016), and the Ministry of Education, Culture, Sports, Science and Technology, Japan (MEXT) to a project on Joint Usage/Research Center, Leading Academia in Marine and Environmental Research (LaMer). Q. Sun thanks support from the NSFC (41376006). Comments from two anonymous reviewers were helpful in improving the original manuscript.

REFERENCES

Chang, P., and A. Isobe, 2003: A numerical study on the Changjiang diluted water in the Yellow and East China Seas. *J. Geophys. Res.*, **108**, 3299, doi:10.1029/2002JC001749.

Chao, S.-Y., 1990: Circulation of the East China Sea, a numerical study. *J. Oceanogr. Soc. Japan*, **46**, 273–295, doi:10.1007/BF02123503.

Chen, C. T. A., and S. L. Wang, 1999: Carbon, alkalinity and nutrient budgets on the East China Sea continental shelf. *J. Geophys. Res.*, **104**, 20 675–20 686, doi:10.1029/1999JC900055.

Chuang, W. S., and W. D. Liang, 1994: Seasonal variability of intrusion of the Kuroshio water across the continental shelf northeast of Taiwan. *J. Oceanogr.*, **50**, 531–542, doi:10.1007/BF02235422.

Ding, R., D. Huang, J. Xuan, B. Mayer, F. Zhou, and T. Pohlmann, 2016: Cross-shelf water exchange in the East China Sea as estimated by satellite altimetry and in situ hydrographic measurement. *J. Geophys. Res. Oceans*, **121**, 7192–7211, doi:10.1002/2016JC011972.

Dyer, K. R., 1979: Estuaries and estuarine sedimentation. *Estuarine Hydrography and Sedimentation: A Handbook*, K. R. Dyer, Ed., Cambridge University Press, 1–18.

Fang, G., Z. Wei, B.-H. Choi, K. Wang, Y. Fang, and W. Li, 2003: Interbasin freshwater, heat and salt transport through the boundaries of the East and South China Seas from a variable-grid global ocean circulation model. *Sci. China*, **46D**, 149–161, doi:10.1360/03yd9014.

Guo, X., H. Hukuda, Y. Miyazawa, and T. Yamagata, 2003: A triply nested ocean model for simulating the Kuroshio—Roles of horizontal resolution on JEBAR. *J. Phys. Oceanogr.*, **33**, 146–169, doi:10.1175/1520-0485(2003)033<0146:ATNOMF>2.0.CO;2.

——, Y. Miyazawa, and T. Yamagata, 2006: The Kuroshio onshore intrusion along the shelf break of the East China Sea: The origin of the Tsushima Warm Current. *J. Phys. Oceanogr.*, **36**, 2205–2231, doi:10.1175/JPO2976.1.

Hirose, N., 2011: Inverse estimation of empirical parameters used in a regional ocean circulation model. *J. Oceanogr.*, **67**, 323–336, doi:10.1007/s10872-011-0041-4.

Hsueh, Y., 2000: The Kuroshio in the East China Sea. *J. Mar. Syst.*, **24**, 131–139, doi:10.1016/S0924-7963(99)00083-4.

——, H. J. Lie, and H. Ichikawa, 1996: On the branching of the Kuroshio west of Kyushu. *J. Geophys. Res.*, **101**, 3851–3857, doi:10.1029/95JC03754.

——, J. R. Schultz, and W. R. Holland, 1997: The Kuroshio flow-through in the East China Sea: A numerical model. *Prog. Oceanogr.*, **39**, 79–108, doi:10.1016/S0079-6611(97)00008-6.

Hu, D.-X., 1994: Some striking features of circulation in Huanghai Sea and East China Sea. *Oceanology of China Seas*, D. Zhou et al., Eds., Springer, 27–38.

Ichikawa, H., and R. C. Beardsley, 2002: The current system in the Yellow and East China Seas. *J. Oceanogr.*, **58**, 77–92, doi:10.1023/A:1015876701363.

Isobe, A., 2000: Two-layer model on the branching of the Kuroshio southwest of Kyushu, Japan. *J. Phys. Oceanogr.*, **30**, 2461–2476, doi:10.1175/1520-0485(2000)030<2461:TLMOTB>2.0.CO;2.

——, 2008: Recent advances in ocean-circulation research on the Yellow Sea and East China Sea shelves. *J. Oceanogr.*, **64**, 569–584, doi:10.1007/s10872-008-0048-7.

——, E. Fujiwara, P.-H. Chang, K. Sugimatsu, M. Shimizu, T. Matsuno, and A. Manda, 2004: Intrusion of less saline shelf water into the Kuroshio subsurface layer in the East China Sea. *J. Oceanogr.*, **60**, 853–863, doi:10.1007/s10872-005-5778-1.

Jacobs, G. A., H. B. Hur, and S. K. Riedlinger, 2000: Yellow and East China Seas response to winds and currents. *J. Geophys. Res.*, **105**, 21 947–21 968, doi:10.1029/2000JC900093.

Kagimoto, T., Y. Miyazawa, X. Guo, and H. Kawajiri, 2008: High resolution Kuroshio forecast system: Description and its applications. *High Resolution Numerical Modelling of the Atmosphere and Ocean*, K. Hamilton and W. Ohfuchi, Ed., Springer, 209–239.

Kalnay, E., and Coauthors, 1996: The NCEP/NCAR 40-Year Reanalysis Project. *Bull. Amer. Meteor. Soc.*, **77**, 437–471, doi:10.1175/1520-0477(1996)077<0437:TNYRP>2.0.CO;2.

Lee, J.-S., and T. Matsuno, 2007: Intrusion of Kuroshio water onto the continental shelf of the East China Sea. *J. Oceanogr.*, **63**, 309–325, doi:10.1007/s10872-007-0030-9.

Lie, H. J., C. H. Cho, J. H. Lee, P. Niiler, and J. H. Hu, 1998: Separation of the Kuroshio water and its penetration onto the continental shelf west of Kyushu. *J. Geophys. Res.*, **103**, 2963–2976, doi:10.1029/97JC03288.

Liu, C., F. Wang, X. Chen, and J.-S. von Storch, 2014: Interannual variability of the Kuroshio onshore intrusion along the East China Sea shelf break: Effect of the Kuroshio volume transport. *J. Geophys. Res. Oceans*, **119**, 6190–6209, doi:10.1002/2013JC009653.

Ma, C., D. Wu, X. Lin, J. Yang, and X. Ju, 2010: An open-ocean forcing in the East China and Yellow seas. *J. Geophys. Res.*, **115**, C12056, doi:10.1029/2010JC006179.

MacCready, P., and W. R. Geyer, 2010: Advances in estuarine physics. *Annu. Rev. Mar. Sci.*, **2**, 35–58, doi:10.1146/annurev-marine-120308-081015.

Mellor, G. L., S. M. Häkkinen, T. Ezer, and R. C. Patchen, 2002: A generalization of a sigma coordinate ocean model and an intercomparison of model vertical grids. *Ocean Forecasting*, N. Pinardi and J. Woods, Ed., Springer, 55–72.

Miyazawa, Y., and Coauthors, 2009: Water mass variability in the western North Pacific detected in a 15-year eddy resolving ocean reanalysis. *J. Oceanogr.*, **65**, 737–756, doi:10.1007/s10872-009-0063-3.

Naimie, C. E., C. A. Blain, and D. R. Lynch, 2001: Seasonal mean circulation in the Yellow Sea—A model-generated climatology. *Cont. Shelf Res.*, **21**, 667–695, doi:10.1016/S0278-4343(00)00102-3.

Oey, L.-Y., Y.-C. Hsin, and C.-R. Wu, 2010: Why does the Kuroshio northeast of Taiwan shift shelfward in winter? *Ocean Dyn.*, **60**, 413–426, doi:10.1007/s10236-009-0259-5.

Pedlosky, J., 1987: *Geophysical Fluid Dynamics.* 2nd ed. Springer-Verlag, 710 pp.

Qiu, B., and N. Imasato, 1990: A numerical study on the formation of the Kuroshio counter current and the Kuroshio branch current in the East China Sea. *Cont. Shelf Res.*, **10**, 165–184, doi:10.1016/0278-4343(90)90028-K.

Ren, J., J. Xuan, Z. Wang, D. Huang, and J. Zhang, 2015: Cross-shelf transport of terrestrial Al enhanced by the transition of northeasterly to southwesterly monsoon wind over the East China Sea. *J. Geophys. Res. Ocean.*, **120**, 5054–5073, doi:10.1002/2014JC010655.

Soeyanto, E., X. Guo, J. Ono, and Y. Miyazawa, 2014: Interannual variations of Kuroshio transport in the East China Sea and its relation to the Pacific decadal oscillation and mesoscale eddies. *J. Geophys. Res. Ocean.*, **119**, 3595–3616, doi:10.1002/2013JC009529.

Su, J. L., 2001: A review of circulation dynamics of the coastal oceans near China (in Chinese). *Acta Oceanol. Sin.*, **23**, 1–16.

Tang, T. Y., and Y. J. Yang, 1993: Low frequency current variability on the shelf break northeast of Taiwan. *J. Oceanogr.*, **49**, 193–210, doi:10.1007/BF02237288.

Taylor, J. R., and S. Sarkar, 2008: Stratification effects in a bottom Ekman layer. *J. Phys. Oceanogr.*, **38**, 2535–2555, doi:10.1175/2008JPO3942.1.

Teague, W. J., G. A. Jacobs, D. S. Ko, T. Y. Tang, K. I. Chang, and M. S. Suk, 2003: Connectivity of the Taiwan, Cheju, and Korea Straits. *Cont. Shelf Res.*, **23**, 63–77, doi:10.1016/S0278-4343(02)00150-4.

Wang, J., and L. Y. Oey, 2016: Seasonal exchanges of the Kuroshio and shelf waters and their impacts on the shelf currents of the East China Sea. *J. Phys. Oceanogr.*, **46**, 1615–1632, doi:10.1175/JPO-D-15-0183.1.

Weatherly, G. L., and P. J. Martin, 1978: On the structure and dynamics of the oceanic bottom boundary layer. *J. Phys. Oceanogr.*, **8**, 557–570, doi:10.1175/1520-0485(1978)008<0557:OTSADO>2.0.CO;2.

Wei, Y., D. Huang, and X.-H. Zhu, 2013: Interannual to decadal variability of the Kuroshio Current in the East China Sea from 1955 to 2010 as indicated by in-situ hydrographic data. *J. Oceanogr.*, **69**, 571–589, doi:10.1007/s10872-013-0193-5.

Wu, C.-R., Y.-C. Hsin, T.-L. Chiang, Y.-F. Lin, and I. F. Tsui, 2014: Seasonal and interannual changes of the Kuroshio intrusion onto the East China Sea Shelf. *J. Geophys. Res. Oceans*, **119**, 5039–5051, doi:10.1002/2013JC009748.

Wu, H., B. Deng, R. Yuan, J. Hu, J. Gu, F. Shen, J. Zhu, and J. Zhang, 2013: Detiding measurement on transport of the Changjiang-derived buoyant coastal current. *J. Phys. Oceanogr.*, **43**, 2388–2399, doi:10.1175/JPO-D-12-0158.1.

Yang, D., B. Yin, Z. Liu, and X. Feng, 2011: Numerical study of the ocean circulation on the East China Sea shelf and a Kuroshio bottom branch northeast of Taiwan in summer. *J. Geophys. Res.*, **116**, C00F05, doi:10.1029/2010JC006526.

——, ——, ——, T. Bai, J. Qi, and H. Chen, 2012: Numerical study on the pattern and origins of Kuroshio branches in the bottom water of southern East China Sea in summer. *J. Geophys. Res.*, **117**, C02014, doi:10.1029/2011JC007528.

Yoshikawa, Y., T. Endoh, T. Matsuno, T. Wagawa, E. Tsutsumi, H. Yoshimura, and Y. Morii, 2010: Turbulent bottom Ekman boundary layer measured over a continental shelf. *Geophys. Res. Lett.*, **37**, L15605, doi:10.1029/2010GL044156.

Zhang, J., S. M. Liu, J. L. Ren, Y. Wu, and G. L. Zhang, 2007: Nutrient gradients from the eutrophic Changjiang (Yangtze River) estuary to the oligotrophic Kuroshio waters and re-evaluation of budgets for the East China Sea Shelf. *Prog. Oceanogr.*, **74**, 449–478, doi:10.1016/j.pocean.2007.04.019.

Zhao, L., and X. Guo, 2011: Influence of cross-shelf water transport on nutrients and phytoplankton in the East China Sea: A model study. *Ocean Sci.*, **7**, 27–43, doi:10.5194/os-7-27-2011.

Zhou, F., H. Xue, D. Huang, J. Xuan, X. Ni, P. Xiu, and Q. Hao, 2015: Cross-shelf exchange in the shelf of the East China Sea. *J. Geophys. Res. Ocean.*, **120**, 1545–1572, doi:10.1002/2014JC010567.